Eur. Phys. J. B **28**, 277–282 (2002)
DOI: 10.1140/epjb/e2002-00230-x

THE EUROPEAN PHYSICAL JOURNAL B

Electron paramagnetic resonance and magnetic susceptibility of rare-earth hydrazone compounds

N. Guskos[1], V. Likodimos[2,a], S. Glenis[1], J. Typek[3], H. Fuks[3], M. Wabia[3], D.G. Paschalidis[4], D. Tossidis[4], and C.L. Lin[5]

[1] Department of Physics, University of Athens, 157 84 Panepistimiopolis, Athens, Greece
[2] Department of Physics, National Technical University, 157 80 Athens, Greece
[3] Institute of Physics, Technical University of Szczecin, Al. Piastow 17, 70 310 Szczecin, Poland
[4] Department of Chemistry, Aristotle University, 54006 Thessaloniki, Greece
[5] Department of Physics, Temple University, Philadelphia, PA 19122, USA

Received 29 April 2002
Published online 31 July 2002 –

Abstract. The magnetic properties of the rare earth molecular compounds with hydrazone ligands containing Nd^{3+}, Gd^{3+}, and Yb^{3+} have been investigated by electron paramagnetic resonance (EPR) and magnetization measurements. For the Gd-compound, partially resolved fine structure due to Gd^{3+} and exchange narrowing effects at low temperatures are observed in the EPR spectra, suggesting, consistent with the EPR and dc magnetic susceptibility, weak antiferromagnetic exchange interactions. Paramagnetic behavior sustained down to low temperatures is derived for Yb^{3+} ions, whereas substantial ferromagnetic exchange coupling is inferred for the lighter Nd^{3+} ions, indicating significant variations of the exchange integrals along the lanthanide series.

PACS. 76.30.-v Electron paramagnetic resonance and relaxation – 76.30.Kg Rare-earth ions and impurities – 75.30.Et Exchange and superexchange interactions

1 Introduction

The distinctive magnetic and spectroscopic properties of trivalent rare earth (R^{3+}) ions and their flexible coordination compounds attract much attention in various research areas ranging from their biological use as spectroscopic and magnetic probes [1] to their utilization in molecular magnetism [2] and the design of device oriented materials [3]. Electron paramagnetic resonance (EPR) has provided precise information on the ground state properties and the strong magnetic anisotropy, which is related to the inherently large orbital contribution of the unfilled $4f$ inner shell of R^{3+} ions [4]. A major limitation, commonly encountered in the EPR study of concentrated R^{3+} compounds required for many practical applications, is the presence of spin-spin interactions that broaden the resonance lines and hinder the resolution of fine structure details [5,6]. However, complications also arise for R^{3+} dopants embedded into various crystal hosts with respect to local lattice distortions [7,8] and their inhomogeneous distribution that may lead to the formation of R^{3+}-R^{3+} pairs or even larger assemblies [8–10]. Studies of the magnetic properties of concentrated R^{3+} molecular compounds could accordingly be of value in elucidating the nature of the intrinsically weak magnetic coupling of R^{3+} ions, provided that sufficient resolution of their resonance spectra is obtained.

In this work, we report on the magnetic properties of three R^{3+} hydrazone molecular compounds $[R(PBH)_2(NO_3)_2]NO_3 \cdot xH_2O$ with R=Nd, Gd, Yb and $x = 0.5, 1.0, 2.0$ respectively, using X-band EPR and magnetization measurements. Partially resolved fine structure due to Gd^{3+} and exchange narrowing effects at low temperatures, rarely observed in the magnetically dense state of most concentrated Gd-compounds, is identified in the EPR spectra, showing, in accord with the EPR and dc magnetic susceptibility, weak antiferromagnetic exchange interactions. Paramagnetic behavior is derived from both EPR and magnetization data for Yb^{3+} ions, whereas ferromagnetic exchange coupling is inferred for Nd^{3+} indicating appreciable variations of the overlap between the localized f-orbitals along the R^{3+} series.

2 Experimental details

Polycrystalline samples of the $[Gd(PBH)_2(NO_3)_2]NO_3{\cdot}H_2O$, $[Yb(PBH)_2(NO_3)_2]NO_3{\cdot}2H_2O$ and $[Nd(PBH)_2(NO_3)_2]NO_3{\cdot}0.5H_2O$ rare earth hydrazone complexes, where PBH corresponds to the 2-pyridinecarboxaldehyde benzoylhydrazone ligand crystallizing as

[a] e-mail: likodimo@gel.demokritos.gr

$PBH{\cdot}H_2O$ with molecular formula $C_{13}H_{13}N_3O_2{\cdot}H_2O$, were prepared, as described elsewhere [11]. Crystal structure determination of the Er-complex shows that the compound crystallizes in the monoclinic $C2/c$ space group stabilized through a complicated hydrogen-bond network, while the members of the homologous series (R=Y, Nd, Eu, Gd, Tb, Dy, Ho, Er, Yb) are also found to belong in the monoclinic system [11]. Each unit cell contains eight molecular units including eight monomeric complex cations, 16 nitrate anions with occupancy of 1/2 and 16 water molecules, eight of which have occupancy of 1/2. The R^{3+} ions are tenfold coordinated with four nitrogen atoms and six oxygen atoms from two tridentate PBH and two bidentate nitrate ligands, respectively. The corresponding coordination polyhedron is best described as a distorted bicapped square antiprism with triclinic local symmetry C_1, lacking any specific symmetry element due to the unequal bond-lengths in the R^{3+}-coordination sphere.

EPR measurements were carried out on powder samples, using a Bruker X-band spectrometer E500 (9.45 GHz) with 100 kHz field modulation and magnetic field sweeps in the range of 0–14 kOe. Temperature dependent EPR measurements were performed using an Oxford flow cryostat and a standard hot air flow system. Magnetic measurements were carried out on the polycrystalline powder samples using a Quantum Design MPMS SQUID magnetometer in the temperature range of 2–300 K and magnetic fields up to 50 kOe. The diamagnetic contribution of the compound was estimated using Pascal's coefficients, while the diamagnetic contribution of the support cell was independently measured and subtracted.

3 Results and discussion

Figure 1 shows representative X-band EPR spectra of $[Gd(PBH)_2(NO_3)_2]NO_3{\cdot}H_2O$ at different temperatures. Despite the magnetically concentrated state of the material, extended fine structure due to Gd^{3+} ions is observed, showing considerable shift of the high-field resonance lines towards higher fields as temperature decreases from 300 to 50 K. Analysis of the powder EPR spectra was carried out for Gd^{3+} ($4f^7$, $^8S_{7/2}$) using the simulation program developed by Weihe [12] that employs exact diagonalization of the energy matrices for each orientation of the magnetic field and takes into account the Boltzmann weighting factor in the resonance line intensity. The zero-field splitting (ZFS) Hamiltonian $H_s = \mu_B S\, g\, H + \sum_{k,q} f_k b_k^q O_k^q$ was accordingly utilized for $S = 7/2$, where the first term describes the Zeeman interaction, O_k^q are the extended Stevens operators, f_k the appropriate scaling factors ($f_2 = 1/3, f_4 = 1/60, f_6 = 1/1260$) and b_k^q the ZFS parameters including both odd and negative-q values pertinent for triclinic local symmetry [13]. The expected small g-anisotropy resulted in negligible effects in the powder lineshape and thus an isotropic g-value of 1.99 was subsequently used.

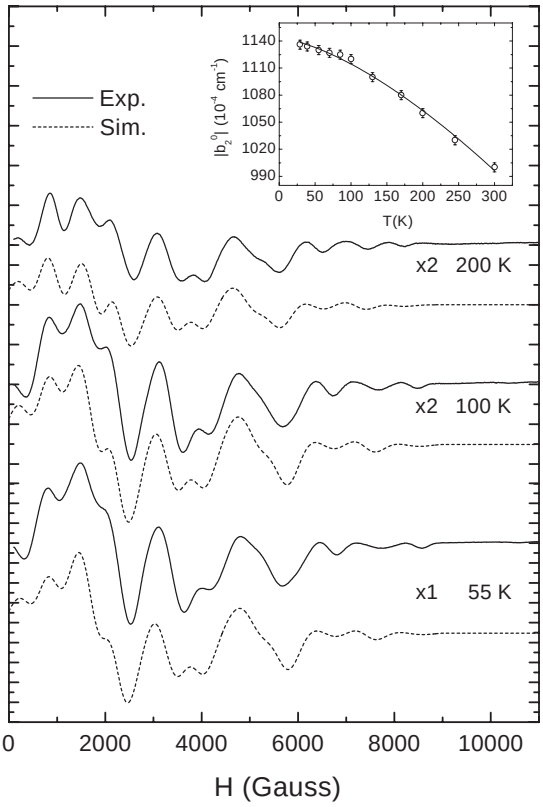

Fig. 1. Experimental Gd^{3+} EPR powder spectra of $[Gd(PBH)_2(NO_3)_2]NO_3{\cdot}H_2O$ (solid lines) in comparison with the simulated ones (dashed lines) using the ZFS parameters (b_2^0, b_4^0) with values (1060, 2) at 200 K, (1120,15) at 100 K, and (1130,20) at 55 K in 10^{-4} cm^{-1} (9.45 GHz). The inset shows the temperature dependence of the axial ZFS parameter fitted to the expression $b_2^0(T) = b_2^0(0)[1 - AT^n]$ with best fit values $b_2^0(0) = 0.1143(3)$ cm^{-1}, $A = 3(2)10^{-5}$ cm^{-1} K^{-1} and $n = 1.5(1)$.

Satisfactory simulations of the EPR powder spectra as a function of temperature were obtained for an axial ZFS parameter that is frequently the dominant component of H_s, with progressively increasing magnitude as temperature decreases (Fig. 1). Better description of the temperature evolution of the relative amplitude of the powder spectrum lines was obtained including a small contribution of b_4^0 ranging from 0.0002 to 0.0020 cm^{-1} as temperature decreases from 200 to 20 K. The magnitude of other second order ZFS parameters was inferred to be an order of magnitude less than b_2^0, within the resolution of the X-band EPR powder spectra. This approximation can be also anticipated for small deviations from the ideal square antiprism local symmetry (D_{4d}), all 10 bond lengths around the R^{3+} site being equal, that leads to the non-vanishing ZFS parameters b_2^0, b_4^0 and b_6^0. The temperature variation of the absolute value of b_2^0 can be empirically described by the nonlinear expression $b_2^0(T) = b_2^0(0)[1 - AT^n]$, with best fit values $b_2^0(0) = 0.1143(3)$ cm^{-1}, $A = 3(2)10^{-5}$ cm^{-1} K^{-1} and $n = 1.5(1)$ (see inset in Fig. 1). Similar behavior has been

observed for the ZFS parameters of Gd^{3+} ions in various hosts [14,15], that is related to the contribution of thermal contraction and vibronic effects. It is worth noting that the absolute value of b_2^0 and the accompanying zero-field splitting is relatively high (the total ZFS is $12b_2^0 = 1.2$ cm^{-1}) making the corresponding molecular compound, which is not water-soluble, attractive for laser applications [16].

The simulation of the EPR powder lineshape was performed employing Gaussian lineshape function with a nearly temperature independent width (half-width at half height) of 780(20) MHz. To explore the broadening of the EPR spectrum the dipole-dipole contribution to the resonance width was roughly estimated in the high temperature limit, using the powder average of the dipolar secular second moment $h^2 M_{2d} = \frac{3}{5} g^4 \mu_B^4 S(S+1) \sum_k r_{jk}^{-6}$, where r_{jk} is the distance between the kth and jth ion taken as origin. The implicated lattice sum was numerically calculated using the crystallographic data [11] over a sphere of 30 Å around the R^{3+} site (8.1361 Å being the shortest r_{jk} distance) yielding a value of $M_{2d} = 4.1 \times 10^5$ (MHz)^2. The dipolar half-width at half height for a Gaussian line would then be given by $\Delta H = \sqrt{2 \ln 2} \sqrt{M_{2d}}$ leading to the value of $\Delta H = 750$ MHz in good agreement with the experimental ΔH values. The integrated EPR intensity I_{EPR}, which corresponds to the spin susceptibility, followed closely the paramagnetic $1/T$ variation in accord with the Boltzmann population of the Gd^{3+} energy levels accounted for by the simulated powder spectra. However, at $T < 15$ K, I_{EPR} increased at a much slower rate than the expected paramagnetic one, as can be inspected in Figure 2. In particular, the temperature dependence of the product of the EPR intensity with temperature $I_{EPR}T$ showed a rapid decrease below 15 K following a Curie-Weiss law with $\Theta = -1.1(1)$ K (see inset in Fig. 2). Most importantly, as temperature decreases, the three outer high-field lines decrease gradually in amplitude and eventually disappear below 5 K, while intensity is transferred to the adjacent resonance line which progressively becomes narrower (Fig. 2). This temperature evolution, which can not be explained by the thermal depopulation of the Gd^{3+} energy levels for either sign of the zero-field splitting parameters, resembles the narrowing effect of the Gd^{3+} fine-structure, thoroughly studied in metallic hosts [18]. In that case, gradual collapse of the Gd^{3+} fine structure occurs mostly through the coupling of the temperature dependent Korringa relaxation rates of adjacent transitions as temperature is raised. Narrowing of the fine structure may be also caused by the exchange interaction of Gd^{3+} moments [19], where the coupling between adjacent resonance transitions arises through an "internal field" term, which shifts the resonance fields while intensity is transferred from one line to the other [18]. The strength of the "internal field narrowing" process is inversely proportional to temperature (Θ/T) and thus for sufficiently low temperatures can produce the collapse of the high field fine structure lines in insulating materials as the present one.

The dc magnetic susceptibility χ, measured at $H = 5$ kOe, follows at high temperatures the Curie behavior of uncorrelated spins with $S = 7/2$ and effective magnetic moment of 7.67 μ_B, close to that expected for free Gd^{3+} ions (7.94 μ_B). At $T < 25$ K, however, a small but distinct decrease of the product χT is observed, which can be fitted to a Curie-Weiss law with $\Theta = -0.49(2)$ K, as illustrated in Figure 3. The field dependence of the magnetization $M(H)$ at 2 and 6 K is shown in the inset of Figure 4. Both $M(H)$ curves are well reproduced by the paramagnetic Brillouin function for $S = 7/2$ with

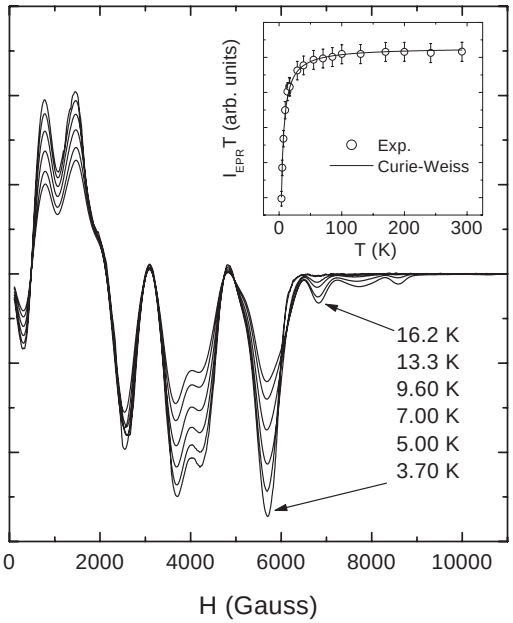

Fig. 2. EPR powder spectra of Gd^{3+} at low temperatures. The inset shows the temperature dependence of the product of EPR intensity with temperature $I_{EPR}T$ and the best fit line to a Curie-Weiss law with $\Theta = -1.1(1)$ K.

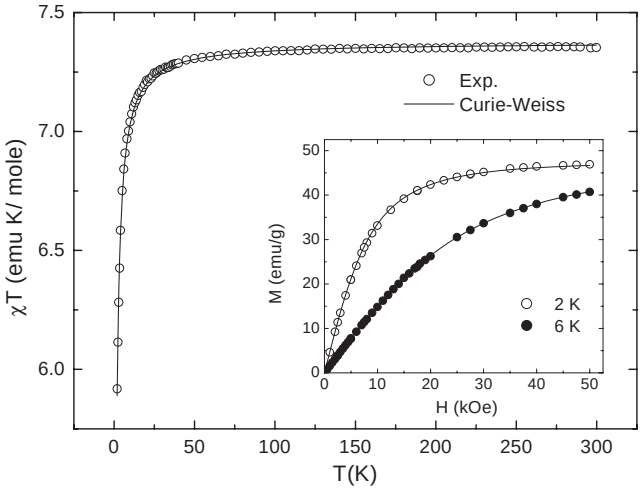

Fig. 3. Temperature dependence of the product χT for $[Gd(PBH)_2(NO_3)_2]NO_3 \cdot H_2O$ at $H = 5$ kOe and the best fit line to a Curie-Weiss law with $\Theta = -0.49(2)$ K. The inset shows the field dependence of the magnetization at 2 and 6 K. Solid lines represent the Brillouin function for $S = 7/2$ with $g = 1.99$.

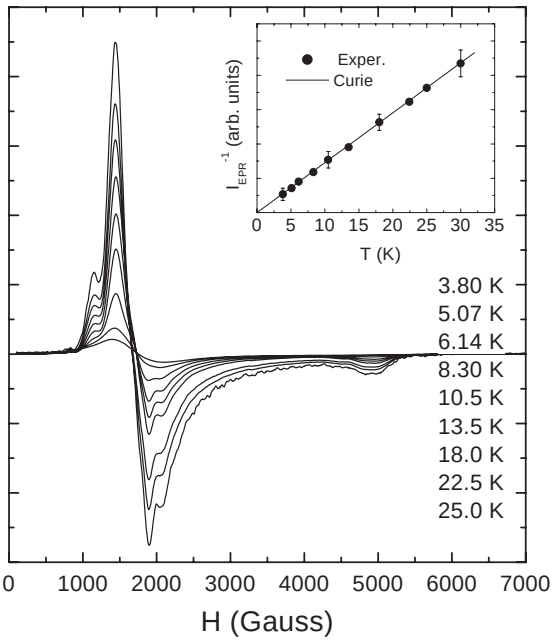

Fig. 4. EPR powder spectra of $[Yb(PBH)_2(NO_3)_2]NO_3{\cdot}2H_2O$ as a function of temperature. The inset shows the temperature dependence of the inverse EPR intensity I_{EPR}^{-1} following the paramagnetic Curie behavior (straight line).

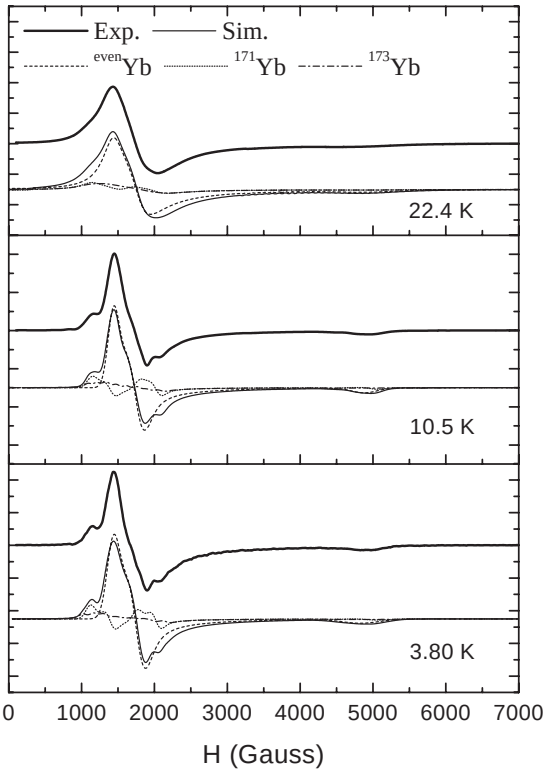

Fig. 5. Simulation of the Yb^{3+} EPR powder spectra at different temperatures. The total simulated EPR spectrum and its components due to the even and odd Yb isotopes are shown below the experimental EPR spectra (9.46 GHz).

$g = 1.99$. The saturation magnetization M_0 thus found is 6.86(1) μ_B/Gd and 6.89(1) μ_B/Gd at 2 and 6 K, respectively, indicating also a small decrease as temperature decreases. Calculation of the paramagnetic susceptibility of Gd^{3+} ions using the ZFS parameters derived from the EPR spectra shows negligible effects for randomly oriented powder samples. Weak antiferromagnetic interactions between Gd^{3+} moments can be thus inferred, consistent with the EPR results.

The temperature dependence of the EPR spectrum for $[Yb(PBH)_2(NO_3)_2]NO_3{\cdot}2H_2O$ is shown in Figure 4. The EPR spectrum consists of an anisotropic powder pattern due to Yb^{3+} ions, which broadens beyond detection at $T > 40$ K due to spin-lattice relaxation. Intense transitions are partially resolved at low fields ($g \approx 4.10$), while a parallel-type powder line of weaker intensity is observed at high fields ($g \approx 1.37$). The eight-fold degenerate $^2F_{7/2}$ ground term of Yb^{3+} ($4f^{13}$) in a site of triclinic symmetry is split by the crystal field (CF) interaction into four Kramers doublets. The temperature variation of the experimental EPR intensity I_{EPR} scales consistently with $1/T$, as expected for a paramagnetic spin doublet at $g\mu_B H \ll kT$ (see inset in Fig. 4). The EPR spectrum was consequently described by the spin-Hamiltonian $H_s = \mu_B S\, g\, H + S\, A\, I$, where $S = 1/2$ is the effective spin describing the two-fold multiplicity of the ground doublet and I the nuclear spin of the Yb odd isotopes (^{171}Yb, $I = 1/2$, ^{173}Yb, $I = 5/2$), while g and A represent the effective-g and hyperfine interaction matrices frequently assumed to be tensors with coincident principal axes provided that no admixture from excited states with different J occurs.

Powder simulation of the EPR spectrum was performed for $S = 1/2$ using the MONOQF program [20], taking into account the two naturally abundant odd isotopes of Yb^{3+} (^{171}Yb, 14.31%, ^{173}Yb, 16.13%) whose hyperfine splitting accounts well for the satellite structure of the low-field EPR spectrum, as shown in Figure 5. Lineshape distortions were progressively observed in the center of the low-field part at $T < 10$ K (Fig. 5), which, however, may be caused by preferable orientation effects induced by the static field along the easy axis of magnetization of loose powder samples [21]. The principal g-values determined from the analysis of the EPR powder spectra as a function of temperature are $g_x = 4.70(3)$, $g_y = 3.85(4)$ and $g_z = 1.40(3)$, yielding an average g-value, defined as $\bar{g} = [(g_x^2 + g_y^2 + g_z^2)/3]^{1/2}$, equal to 3.60. The absolute values of the hyperfine principal components were found to be $A_x = 1300(50)$ MHz, $A_y = 1100(50)$ MHz, $A_z = 350(20)$ MHz for ^{171}Yb, and $A_x = 330(30)$ MHz, $A_y = 250(50)$ MHz, $A_z = 100(20)$ MHz for ^{173}Yb, within the resolution of the X-band powder spectra. These values are close to those predicted by $\frac{g_i}{A_i} = \frac{g_J}{A_J}(i = x, y, z)$, where g_J (1.141) is the Lande g-factor of the $^2F_{7/2}$ ground term and A_J the magnetic hyperfine constants of ^{171}Yb(+887.2 MHz) and ^{173}Yb(−243.3 MHz), indicating relatively small misalignment between g and A [22].

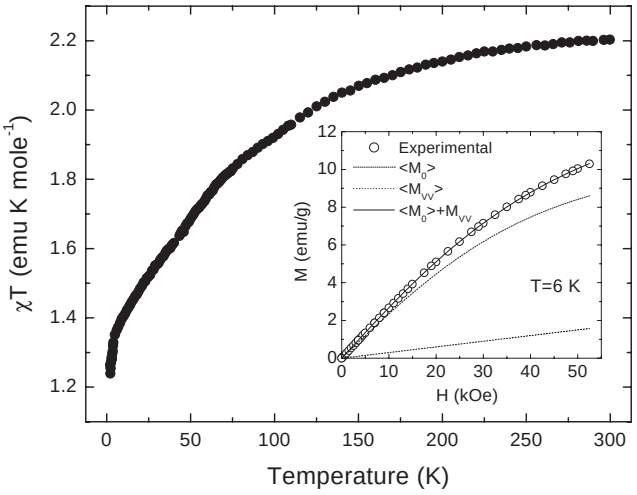

Fig. 6. Temperature dependence of χT for $[Yb(PBH)_2(NO_3)_2]NO_3{\cdot}2H_2O$ measured at $H = 5$ kOe. The inset shows the field dependence of the magnetization at 6 K in comparison with the theoretical curve and the individual components $\langle M_0 \rangle$ and M_{VV} with best fit value of $\chi_{VV} = 0.0253(5)$ emu/mole.

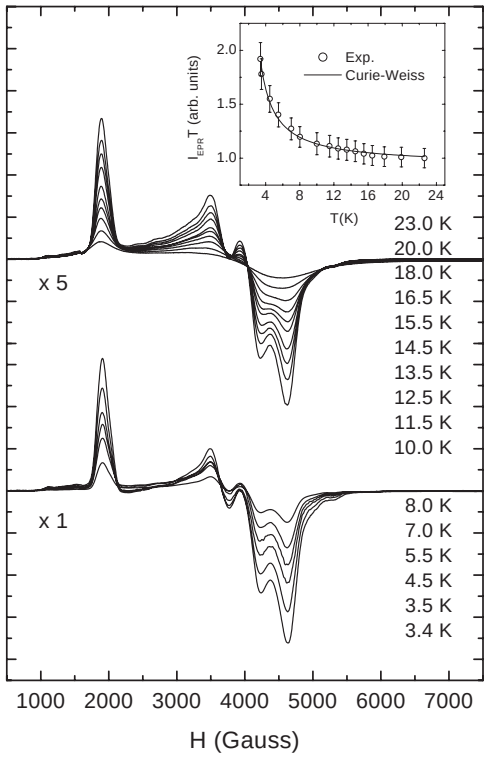

Fig. 7. EPR powder spectra of $[Nd(PBH)_2(NO_3)_2]NO_3{\cdot}0.5H_2O$ as a function of temperature (9.46 GHz). The inset shows the temperature dependence of the product $I_{EPR}T$ and the best fit line to a Curie-Weiss law with positive $\Theta = 1.7(1)$ K.

The resonance width ΔH_i $(i = x, y, z)$ was found to increase from 500–550 MHz at 3.8 K to 1100–1150 MHz at 22.4 K. An estimate of the powder average of the secular dipolar moment M_{2d} using $g = 3.60$ and the crystallographic distances [11], results in $M_{2d} = 2.03 \times 10^5$ $(\text{MHz})^2$, which corresponds to the dipolar Gaussian width of $\Delta H \approx 530$ MHz. Although this value represents only a rough estimate of the anisotropic dipolar width, it turns out to be in good agreement with the low-temperature experimental ΔH values reflecting the spin-spin dependent residual width.

The product of the dc magnetic susceptibility with temperature χT of Yb-compound, measured in magnetic field $H = 5$ kOe, yields an effective moment of 4.20(1) μ_B at 300 K approaching the theoretical value of 4.54 μ_B for free Yb^{3+}. As temperature decreases, χT decreases reflecting the gradual depopulation of the excited CF states, as shown in Figure 6. An abrupt reduction of χT is observed at $T < 10$ K, indicating a dominant contribution of the ground Kramers doublet. The experimental $\chi(T)$ in the temperature range of 2–10 K was accordingly fitted to the Curie law, where C is the Curie constant and χ_{VV} is the temperature independent Van Vleck contribution arising from the excited CF states. An accurate description of the experimental data was thus obtained for $C = 1.21(1)$ emu K/mole and $\chi_{VV} = 0.025(2)$ emu/mole. The Curie constant corresponds to an effective moment of 3.11(3) μ_B and an average g-value for the ground doublet $g = 3.60(3)$, in excellent agreement with the EPR g-value. The field dependence of the magnetization $M(H)$ measured at 6 K is shown in the inset of Figure 6. The $M(H)$ data were subsequently analyzed according to the expression $M(H) = \langle M_0 \rangle + M_{VV}$ [23], where $\langle M_0 \rangle$ is the angle-averaged magnetization of the ground doublet and M_{VV} is the Van Vleck contribution approximated by $\chi_{VV}H$. The $\langle M_0 \rangle$ term was numerically calculated from the corresponding Brillouin function for $S = 1/2$ with $g = (g_x^2 \sin^2\theta\cos^2\phi + g_y^2 \sin^2\theta \sin^2\phi + g_z \cos^2\theta)^{1/2}$ determined from the principal g-values found from the EPR spectra, leaving χ_{VV} as the only adjustable variable. An accurate description of $M(H)$ was obtained for $\chi_{VV} = 0.0253(5)$ emu/mole (see inset in Fig. 6), that practically coincides with the value determined from the magnetic susceptibility. Although the anisotropy of the Van Vleck term imposed by the CF energy level scheme is thus neglected, a plausible assumption for a polycrystalline sample, both EPR and magnetic measurements suggest predominant paramagnetic response of Yb^{3+}. Consequently, suppressed exchange interactions may be inferred for the heavier R^{3+} ions, whereas enhanced exchange coupling could be anticipated for the light R^{3+} ions characterized by extended f-orbitals.

To this aim, X-band EPR measurements were carried out as a function of temperature on the $[Nd(PBH)_2(NO_3)_2]NO_3{\cdot}0.5H_2O$ compound containing the lighter Nd^{3+} ions in the R^{3+} hydrazone series [11]. Figure 7 shows the temperature dependence of the Nd^{3+} EPR spectrum, which broadens excessively at $T > 25$ K due to fast spin-lattice relaxation. The EPR powder spectrum consists mainly of four intense transitions at $g \approx 3.55$, 1.86, 1.65 and 1.45, whose relative intensities vary proportionally and gradually broaden as temperature increases. The ten-fold degenerate $^4I_{9/2}$ ground term of Nd^{3+} $(4f^3)$

in a site of low symmetry is split by the CF interaction into five Kramers doublets. Owing to the rapid relaxation of the excited states, EPR is usually observable only between the Zeeman components of the ground doublet described by an effective spin $S = 1/2$. Provided that there is a single crystallographic site as in the present case, the usual three-line EPR powder pattern [20], corresponding to the three principal components of the g-tensor of the Nd^{3+} ground doublet, is expected in contrast with the experimental EPR spectrum. Contributions from the hyperfine structure of the two odd isotopes of Nd^{3+} (^{143}Nd, $I = 7/2$, 12.17%, ^{145}Nd, $I = 7/2$, 8.3%) are minor in the final EPR powder spectrum due to their low abundance, accounting solely for the weak satellite lines on both spectral wings. The presence of Nd^{3+}-Nd^{3+} pair interactions may be thus inferred for the Nd-hydrazone complex, although both Gd^{3+} and Yb^{3+} EPR spectra show the features expected within a single-ion picture. Simulations of the EPR spectrum on the basis of dipolar coupled Nd^{3+}-Nd^{3+} dimers at interionic distances of 8.1 Å doubles all resonance lines with a relatively small splitting, indicating a more complicated interaction scheme between Nd^{3+} ions involving both exchange and dipole-dipole interactions as well as the relative orientation of the g-tensors of the magnetically inequivalent Nd^{3+} sites. Evidence for the existence of exchange coupling between Nd^{3+} ions is directly provided by the product of the EPR intensity with temperature $I_{EPR}T$, which increases considerably upon decreasing temperature following a Curie-Weiss law with positive $\Theta = 1.7(1)$ K (see inset in Fig. 7). Substantial ferromagnetic exchange interactions can be accordingly deduced for Nd^{3+}, indicating significant changes of the R^{3+} exchange integrals along the homologous lanthanide compounds.

4 Conclusions

In summary, the rare earth hydrazone compounds $[R(PBH)_2(NO_3)_2]NO_3 \cdot xH_2O$ with R=Nd, Gd, Yb and $x = 0.5$, 1.0, 2.0 respectively, were studied by EPR and magnetization measurements. Partially resolved fine structure due to Gd^{3+}, rarely reported for most magnetically concentrated Gd-compounds, is observed in the X-band EPR spectra of the Gd-compound, dominated by a large, temperature dependent axial zero-field splitting. Significant narrowing of the Gd^{3+} fine structure is observed at low temperatures ($T < 10$ K), implying an internal field narrowing process due to Gd^{3+}exchange coupling. The latter result is further corroborated by the temperature dependence of both the EPR intensity and dc susceptibility that indicate weak antiferromagnetic interactions between Gd^{3+} ions. For the Yb-compound, the ground Kramers doublet of Yb^{3+} is characterized by strongly anisotropic g and hyperfine tensors, though paramagnetic behavior is derived down to low temperatures from both EPR and magnetization measurements, implying suppressed exchange interactions for the heavier R^{3+} ions. On the other hand, appreciable ferromagnetic coupling is inferred from EPR for the lighter Nd^{3+} ions indicating significant variations of the R^{3+} exchange integrals mediated through the hydrogen bond network for the lanthanide series.

References

1. J.C. Bünzli, N. André, M. Elhabiri, G. Muller, C. Piguet, J. Alloys Comp. **303**, 66 (2000)
2. A. Dei, D. Gatteschi, J. Pécaut, S. Poussereau, L. Sorace, K. Vostrikova, C. R. Acad. Sci. Paris, Chimie **4**, 135 (2001)
3. V.S. Mironov, Y.G. Galyametdinov, A. Ceulemans, C. Görller-Warland, K. Binnemans, Chem. Phys. Lett. **345**, 132 (2001)
4. A. Abragam, B. Bleaney, *Electron Paramagnetic Resonance of Transition Ions* (Clarendon Press, Oxford, 1970)
5. C. Filip, C. Kessler, F. Balibanu, P. Kleeman, A. Darabont, L.V. Giurgiu, M. Mehring, Physica B **222**, 16 (1996)
6. V. Likodimos, N. Guskos, M. Wabia, J. Typek, Phys. Rev. B **58**, 8244 (1998)
7. S.K. Misra, S.I. Andronenko, Phys. Rev. B **53**, 11631 (1996)
8. E. Antic-Fidanchev, J. Hölsä, M. Lastusaari, A. Lupei, Phys. Rev. B **64**, 195108 (2001)
9. O. Guillot-Noël, V. Mehta, B. Viana, D. Gourier, M. Boukhris, S. Jandl, Phys. Rev. B **61**, 15338 (2000)
10. B.Z. Malkin, A.M. Leushin, A.I. Iskhakova, J. Heber, M. Altwein, K. Moller, I.I. Fazlizhanov, V.A. Ilanov, Phys. Rev. B **62**, 7063 (2000)
11. D.G. Paschalidis, I.A. Tossidis, M. Gdaniec, Polyhedron **19**, 2629 (2000); D.G. Paschalidis *et al.* (private communication)
12. C.J.H. Jacobsen, E. Pedersen, J. Villadsen, H. Weihe, Inorg. Chem. **32**, 1216 (1993)
13. C. Rudowicz, H.W.F. Sung, Physica B **300**, 1 (2001)
14. N. Guskos, J. Kuriata, T. Rewaj, Acta Phys. Pol. A **81**, 659 (1992)
15. X. Gratens, S. Isber, S. Charar, C. Fau, M. Averous, S.K. Misra, Z. Golacki, M. Ferhat, J.C. Tedenac, Phys. Rev. B **55**, 8075 (1997)
16. K.J. Guedes, K. Krambrock, J.Y. Gesland, J. Phys. Cond. Matt. **11**, 7211 (1999)
17. J.H. Van Vleck, Phys. Rev. B **74**, 1168 (1948)
18. S.E. Barnes, Adv. Phys. **30**, 801 (1981)
19. P. Urban, D. Davidov, B. Elschner, T. Plefka, G. Sperlich, Phys. Rev. B **12**, 72 (1975)
20. J.R. Pilbrow, *Transition-Ion Electron Paramagnetic Resonance* (Clarendon Press, Oxford, 1990)
21. J. Hulliger, L. Zoller, J.H. Ammeter, J. Magn. Res. **48**, 512 (1982)
22. J.R. Pilbrow, M.R. Lowrey, Rep. Prog. Phys. **43**, 433 (1980)
23. J.A. Hodges, P. Bonville, A. Forget, M. Rams, K. Królas, G. Dhalenne, J. Phys. Cond. Matt. **13**, 9301 (2001)